ELSEVIER

Surface and structural properties of zirconia-supported vanadium oxide Influence of the preparation pH

Mario Valigi[a,*], Delia Gazzoli[a], Giovanni Ferraris[a], Sergio De Rossi[a], Roberto Spinicci[b]

[a] *Istituto di Metodologie Inorganiche e dei Plasmi (IMIP), CNR e Dipartimento di Chimica, Università di Roma 'La Sapienza', Piazzale Aldo Moro, 5, I-00185 Rome, Italy*
[b] *Dipartimento di Energetica, Università di Firenze, via S. Marta, 3, I-50139 Florence, Italy*

Received 30 July 2004; received in revised form 30 September 2004; accepted 7 October 2004
Available online 19 November 2004

Abstract

Zirconia-supported vanadium oxide catalysts were prepared by equilibrium adsorption in acid (pH 2.7) or basic (pH 10) conditions using hydrous zirconium oxide and an aqueous solution of ammonium metavanadate. The samples, containing vanadium up to 22.24 wt.%, heated at 823 K for 5 h in air, were studied as prepared and after leaching with an ammonia solution by X-ray diffraction, X-ray photoelectron spectroscopy, diffuse optical reflectance, surface area measurements and pore size distribution determination.

Owing to the microporous support and to the different condensation degree of the vanadium species, the precursors showed distinct features. The diversity persisted after heating and became more evident at increasing vanadium content. At similar vanadium loading, the fraction in a dispersed state and thus interacting with the support was higher in samples at pH 10 than in those prepared at pH 2.7. For pH 2.7 samples, heating favoured the formation of V_2O_5 and of ZrV_2O_7. The interaction between the vanadium dispersed species and the zirconia surface strongly affected the texture, sintering and phase transition of the support.
© 2004 Elsevier B.V. All rights reserved.

1. Introduction

Vanadium oxide is a well-known catalyst for many reactions of industrial interest and its role in supported catalysts has been recently reviewed [1]. In spite of the great efforts, some problems related to the active sites (isolated or polymeric species) are still under debate [2]. Some of these problems can be clarified by characterizing the precursor state in detail [3].

Several oxides have been considered as a support, including ZrO_2 [2,4–12]. Although preformed ZrO_2 is often used as support, amorphous hydrous zirconium oxide can yield systems with particular properties [13,15].

For catalyst preparation, among the wet deposition procedures, the equilibrium adsorption method in principle allows a uniform distribution of the active phase. In our

laboratory, we used this method to investigate zirconia-based catalysts containing various Me [Me = Cr(VI), Mo(VI), W(VI)] species starting from hydrous zirconium oxide [13,16,17]. These experiments underlined the solution pH as a determinant factor because it affects the adsorption properties of the solid and can control the predominant Me-ionic species in solution. Controlling the predominant Me-ionic species in solution is especially important for vanadium, which can be present in solution as small ionic species at basic pH or as large polyoxoanions in acid conditions. Another advantage of the equilibrium adsorption method is that it provides at a given pH precursors with similar vanadium loading but with different degree of dispersion of the adsorbed species. Because hydrous zirconium oxide is microporous, the large polyoxoanions suffer diffusion limitation in the micropores, and may therefore be adsorbed only on the external surface of the support [18,19].

After deposition of the catalytic active species, the precursor is heated. Samples prepared with preformed ZrO_2

* Corresponding author. Tel.: +39 06 49913377; fax: +39 06 490324.
E-mail address: mario.valigi@uniroma1.it (M. Valigi).

undergo heat-induced changes mostly in the supported species, whereas those obtained from hydrous ZrO_2 undergo changes also in the textural and morphological properties of the support. Rather than being a drawback these changes are actually advantageous because they allow one to investigate properties of the active species-support interaction that are usually disregarded, for example its effect on support properties such as crystallization and sintering.

In the present paper, we studied vanadium oxide supported on zirconia catalysts prepared by equilibrium adsorption at two pH values. To investigate the predominant type and degree of dispersion of the vanadium species as well as the structural and textural features of the support, we examined the catalysts obtained from precursors having similar loading but different dispersion degree.

2. Experimental

2.1. Samples preparation

The starting material was hydrous zirconium oxide prepared by bubbling a stream of ammonia-saturated N_2 into a $ZrOCl_2$ solution for 72 h, as already reported [14]. After separation, the solid was washed (Cl^- negative test in the solid), and dried at 383 K, for 24 h. The obtained hydrous zirconium oxide was microporous (specific surface area: $330\,m^2\,g^{-1}$) and amorphous to X-ray. It was designated as $ZrO_2(383)$ and used to prepare the vanadium-containing samples. They were obtained by suspending an amount of $ZrO_2(383)$ in a relatively large volume of V(v) aqueous solution (from NH_4VO_3, Fluka) at a given pH (10 or 2.7) fixed by NH_4OH or HNO_3. The suspension was shaken for 72 h at room temperature to equilibrate the system. The solid was filtered from the liquid fraction, dried at 383 K for 24 h and finally heated in air at 823 K, 5 h. The samples were designated as ZVx,y where x stands for the vanadium content as wt.% (metal) and y the pH value (Table 1). Two fractions of $ZrO_2(383)$, contacted with vanadium-free aqueous solutions at pH 10 or 2.7, were submitted to similar treatments (shaking, filtering, heating at 823 K) and were indicated as $ZrO_2(823)y$.

Pure V_2O_5 and ZrV_2O_7 were used as reference compounds. The vanadium pentoxide was obtained by decomposing NH_4VO_3 (Fluka) in air at 873 K for 3 h. ZrV_2O_7 was prepared from a mixture of V_2O_5 and $ZrO_2(383)$ heated in air at 983 K following the procedure described by Sanati et al. [20]. To avoid an incomplete reaction, V_2O_5 was added in a slightly larger amount than the stoichiometric ratio. The amount of ZrO_2 in $ZrO_2(383)$ was evaluated by heating the hydrous oxide, in air, up to 1083 K in a thermogravimetric apparatus. After heating the mixture, the pentoxide in excess was removed with an ammonia solution using a procedure similar to that applied for determining V_2O_5 in the samples. The X-ray diffraction patterns of V_2O_5, and ZrV_2O_7 reference compounds, corresponded to those reported in the literature [21,22].

Table 1
Specific surface area, S; crystalline phases; fraction of tetragonal modification, f_t; vanadium content leached by ammonia, $V(NH_3)$; and remaining in the solid residue, V_{sr}; for zirconia-supported vanadium oxide samples after heating at 823 K for 5 h, in air

Samples[a]	S ($m^2\,g^{-1}$)	Phases[b]	f_t	$V(NH_3)$ (wt.%)	V_{sr} (wt.%)
$ZrO_2(823)$	49	m, t	0.23	0.0	0.0
ZV0.27,10	51	m, t	0.44	0.00	0.27
ZV0.50,10	85	m, t	0.54	0.00	0.50
ZV0.99,10	79	m, t	0.43	0.08	0.91
ZV1.73,10	93	m, t	0.60	0.45	1.28
ZV1.99,10	95	m, t	0.78	0.24	1.75
ZV3.10,10	105	m, t	0.85	0.50	2.60
ZV5.14,10	138	m, t	0.71	1.18	3.96
ZV5.28,10	124	m, t	0.77	1.72	3.56
ZV5.72,10	119	m, t	0.75	1.96	3.76
ZV6.41,10	114	m, t	0.85	2.05	4.36
ZV6.91,10	118	m, t	0.92	2.07	4.84
ZV0.50,2.7	62	m, t	0.41	0.14	0.36
ZV1.31,2.7	78	m, t	0.42	0.37	0.94
ZV1.40,2.7	90	m, t	0.63	0.36	1.04
ZV2.63,2.7	97	m, t	0.62	0.61	2.02
ZV2.82,2.7	98	m, t	0.77	0.66	2.16
ZV3.74,2.7	49	m, t, Z	0.77	1.10	2.64
ZV4.74,2.7	52	m, t, Z	0.74	1.12	3.62
ZV7.83,2.7	41	m, t, Z	0.84	1.85	5.98
ZV7.94,2.7	42	m, t, Z	0.77	1.73	6.21
ZV8.32,2.7	39	m, t, Z, V_2O_5	0.79	2.94	5.38
ZV22.24,2.7	28	m, t, Z, V_2O_5	0.78	14.5	7.74

[a] For designation of samples see text.
[b] m = monoclinic ZrO_2, t = tetragonal ZrO_2, Z = ZrV_2O_7.

2.2. Chemical analysis

The vanadium content was determined by atomic absorption after dissolving the sample in a concentrated HF solution, and subsequent dilution [23]. The standard solution (Fluka 1000 ppm) contained ZrO_2, dissolved in HF, in a concentration similar to that of the samples.

Because V_2O_5 is soluble in ammonia solution [24], a portion of each sample (typically 70 mg) was contacted with a hot ammonia solution (about 20 ml, $2\,mol\,l^{-1}$) in a closed vessel for 30 min, under stirring. The solid was then separated and leached three times. The liquid fractions were collected and the vanadium content was determined by atomic absorption. ZrV_2O_7 washed in similar manner released no detectable vanadium. The vanadium remaining in the solid residue, V_{sr}, was calculated for each sample from the total vanadium content, V, and the vanadium content leached with an ammonia solution, $V(NH_3)$, as $V_{sr} = V - V(NH_3)$, Table 1.

2.3. X-ray diffraction determinations

XRD patterns in the 2θ angular range from 5 to $60°$ were obtained by a Philips diffractometer using a 1732/10 generator and Cu Kα (Ni-filtered) radiation. The fraction of

tetragonal zirconia, f_t, was evaluated by the formula

$$f_t = \frac{A_t(101)}{A_t(101) + A_m(111) + A_m(1\,1\,\bar{1})}$$

where $A_t(1\,0\,1)$ stands for the area of the tetragonal peak $(1\,0\,1)$, and $A_m(1\,1\,1)$ and $A_m(1\,1\,\bar{1})$ for the areas of the monoclinic peaks $(1\,1\,1)$ and $(1\,1\,\bar{1})$. The tetragonal and monoclinic peaks were resolved by considering them symmetric. Repeated measurements of the same sample showed that the uncertainty in the f_t values was ± 0.05.

2.4. Texture analysis

Surface area measurements (BET method) and pore size analysis (BJH method, using the adsorption branch of the isotherm) were obtained by N_2 adsorption–desorption at 77 K using a ASAP 2010 Micromeritics apparatus. The samples were outgassed under vacuum for 2 h at 473 K, before the measurement.

Because ZrV_2O_7 and V_2O_5 exhibited narrow XRD reflections, the contribution of these phases to the specific surface area (S) of the samples was considered negligible, Table 1. For each sample the specific surface area of zirconia, $S(ZrO_2)$, was obtained by the following formula

$$S(ZrO_2) = \frac{S}{1 - (\%V/100) \times 90.94/50.94}$$

where 50.94 is the atomic molar mass of V and 90.94 the half of the molecular molar mass of V_2O_5. The calculated values are a first approximation because all vanadium is considered present as V_2O_5.

2.5. Diffuse reflectance spectroscopy

UV–vis spectra were recorded under ambient conditions in the range 2500–200 nm on a Cary 5E spectrophotometer with the diffuse reflectance attachment by Varian Win UV software. Halon was used as reference. The Kubelka–Munk function, $F(R_\infty)$, was obtained from reflectance.

2.6. X-ray photoelectron spectroscopy analysis

XPS spectra were collected by a Leybold-Heraeus LHS10 spectrometer in FAT mode (50 eV pass energy) with Mg Kα radiation (10 kV/20 mA) at a pressure lower than 10^{-9} Torr. The samples, reduced to fine powders, were manually pressed onto a gold plate attached to the sample rod. The O 1s + V 2p, C 1s and Zr 3d regions were sequentially acquired by a computer. Data analysis involved X-ray satellite removal, non-linear Shirley-type background subtraction and curve-fitting by Esca Tools 4.2 software (Surface Interface Inc., Mountain View, California).

The satellite structure of the O 1s peak seen in the O 1s + V 2p region, due to the $K\alpha_{3,4}$ intensities of the non-monochromatized X-ray anode, was removed according to

reported parameters [25]. Vanadium peak areas were determined by integrating the V $2p_{3/2}$ contribution after appropriate background subtraction. Electron binding energies were referenced to the Zr $3d_{5/2}$ peak at 182.5 eV.

To assess a quantitative relationship between the XPS peak intensity ratio and surface morphology, the experimental results were compared with theoretical values obtained by specific models, chosen according to the chemistry of the system components [26]. The model proposed by Kerkhof–Moulijn (K–M) [27] and the 'non-attenuating overlayer over a semi-infinite support' representation [28] were considered. The K–M model describes the supported species 'promoter', p, as uniformly distributed on the surface of the porous support, s, including the internal surface. The support consists of stacked sheets with thickness, t, evaluated by the sample surface area (S) and the density (d) of the carrier: $t = 2/Sd$. The intensity ratio is given as:

$$\frac{I_P}{I_s} = \frac{D_P}{D_s} \frac{\sigma_p}{\sigma_s} \frac{\beta_1}{2} \frac{[1 + \exp(-\beta_2)]}{[1 - \exp(-\beta_2)]} \frac{n_p}{n_s}$$

where D is the instrumental efficiency factor; n_p/n_s the promoter/support atomic ratio; $\beta_1 = t/\lambda_{ss}$, $\beta_2 = t/\lambda_{ps}$ where λ_{ss} and λ_{ps} refer to the escape depth of electron from promoter and support respectively through the support; and σ_s, σ_p are the cross sections. The 'non-attenuating overlayer over a semi-infinite support' model describes the system as a non-attenuating atomically dispersed promoter, p, with surface density s_p over a planar semi-infinite support, s:

$$\frac{I_p}{I_s} = \frac{D_p}{D_s} \frac{\sigma_p}{\sigma_s} \frac{s_p}{\rho_s \lambda_{ss}}$$

where ρ_s = support density (atoms cm^{-3}) and the other quantities previously defined.

The intensity ratios were calculated from: $d = 5.5$ g cm^{-3}; $\rho_s = 0.27 \times 10^{23}$ atoms cm-3; theoretical σ values proposed by Scofield [29] [V $2p_{3/2}$: $\sigma = 6.33$; Zr 3d: $\sigma = 7.3$]; λ values according to Seah [30] (V: $\lambda_{ps} = 1.66$ nm, Zr: $\lambda_{ss} = 2.0$ nm); the instrumental efficiency factor dependent on kinetic energy, (KE), as: $D = (KE)^{-0.82}$ [31].

3. Results and discussion

The properties of ZV$x,y$ samples depend on the preparation conditions. As discussed in detail [19], the uptake of vanadium species depends on the pH of the solution in contact with the microporous zirconia. The point of zero charge of preformed zirconium oxide is in the range 6–8 [32]. For hydrous zirconium oxide, a higher value (9.4) was recently measured [33]. At pH 2.7 the adsorbent surface is positively polarized favoring the adsorption of the large $H_zV_{10}O_{28}^{(6-z)-}$ (where z may be 0, 1 or 2) polyoxoanions present in the solution. Because these large polyanions are comparable to the support micropores in size they can penetrate only a limited thickness of the support grains and are therefore adsorbed on only a fraction of the support
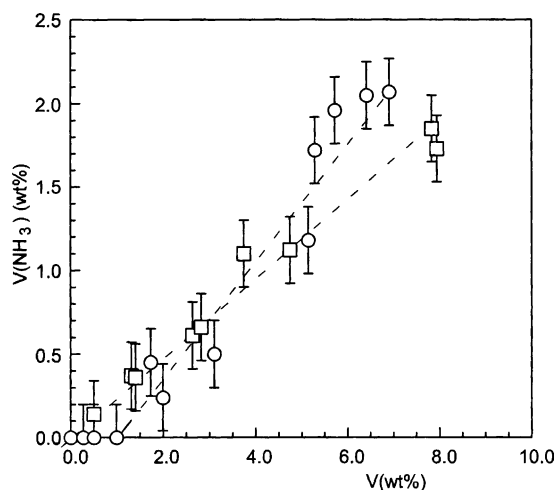
Fig. 1. Vanadium content leached with an ammonia solution, $V(NH_3)$ (wt.%), as a function of the total vanadium content, V (wt.%). ($\bigcirc$) ZVx,10; ($\square$) ZVx,2.7.

Fig. 2. (a) XPS intensity ratios, I_V/I_{Zr}, as a function of the surface vanadium concentration, V/atoms nm^{-2}. ($\bigcirc$) ZVx,10; ($\square$) ZVx,2.7. (b) XPS intensity ratios, I_V/I_{Zr}, vs. the promoter support atomic ratio, p/s. Dashed line: calculated value (K–M model). (c) XPS intensity ratios, I_V/I_{Zr}, vs. the surface vanadium concentration, V/atoms nm^{-2}. Solid line: calculated values (non-attenuating overlayer model).

surface [19]. At pH 10, the small vanadium anions ($V_2O_7^{4-}$) are predominantly present in solution and, although their adsorption is hindered by the negative polarized surface of the adsorbent, they can diffuse through the support micropores and reach practically the whole surface of the $ZrO_2(383)$ grains. For similar vanadium loading, the vanadium species taken up at pH 10 therefore have a higher dispersion degree than those adsorbed at pH 2.7. During the subsequent heating at 823 K, for 5 h in air, the support and the adsorbed species both undergo physical and chemical processes (dehydration, crystallization, decomposition, interaction). Owing to the initial diversity, the two sets of samples, at similar vanadium content, differ in the fraction of the various vanadium species and in the support properties. The X-ray patterns of ZVx,10 samples showed no reflections other than the monoclinic and tetragonal ZrO_2, Table 1. Nor did the ZVx,2.7 samples with $x < 3.74$, but starting from this vanadium content the lines of ZrV_2O_7 and, for the most concentrated, V_2O_5 appeared.

The two series of samples differed in the amount of vanadium rinsable with an ammonia solution. All the ZVx,2.7 samples but only ZVx,10 from $x > 0.99$ contained soluble vanadium, Fig. 1. Except for the most concentrated ZVx,2.7 samples, for which X-ray diffraction revealed the pentoxide, for all the other samples, the rinsable vanadium came from V_2O_5 in the form of small crystallites or vanadia-like amorphous polymers, or both (Table 1).

XPS confirmed the different dispersion degree of the vanadium species for the two series of samples. The experimental intensity ratios V 2p$_{3/2}$/Zr 3d, I_V/I_{Zr}, as a function of the apparent vanadium surface concentration, continuously increased for ZVx,10 samples, whereas for ZVx,2.7 samples, the intensity ratios increased with a decreasing slope (Fig. 2 (a)). For the ZVx,10 samples, the K–M model satisfactory reproduced the experimental values (Fig. 2 (b)) because the sample set retained a high surface area. Hence the support consisting of stacked sheets of thick-

ness t was thin enough to allow the passage of the electrons coming from the promoter adsorbed on its internal surfaces.

The agreement between the experimental and calculated intensity ratios indicated a high dispersion of the vanadium species on the zirconia surface. For the ZVx,2.7 samples, the calculated values agreed with the experimental values, when we applied the non-attenuating overlayer over a semi-infinite support model. This model was more appropriate than the K–M model for representing the sample morphology because the decrease in the surface area, at increasing vanadium content, led to a thick material, whose t values were larger than λ values, ($t \sim 7.0$ nm; $\lambda \sim 2.0$ nm). However, the agreement appeared to be satisfactory only for the dilute samples; at higher vanadium content the experimental values were much lower than the calculated ones, Fig. 2 (c). The deviation from the linear behaviour indicates that the surface species agglomerated as ZrV_2O_7 or V_2O_5 or both.

The foregoing conclusions received support from the analysis of the reflectance spectra. The reflectance spectrum of ZrV_2O_7, was characterized by absorption bands at 25,000, 33,000 and 44,000 cm^{-1} (Fig. 3). V_2O_5 showed absorptions at 21,000, 31,000 and 42,000 cm^{-1} as reported in the literature [11]. The $ZrO_2(823)10$ and $ZrO_2(823)2.7$ samples had similar spectra showing an absorption maximum at $\sim$44,000 cm^{-1} (Fig. 3).

The strong absorption bands between 18,000 and 40,000 cm^{-1}, observed for ZVx,10 and ZVx,2.7 samples, Figs. 4 and 5, originate from charge transfer transitions ($O^{2-}_{(2p)} \rightarrow V^{5+}_{(3d)}$) [34], insofar as ZrO_2 absorbs over 42,000 cm^{-1}. The charge transfer bands are strongly influenced by the coordination and by the condensation degree of the vanadium species [35–37], the latter affecting also the band edge [11,38]. Hence, in principle, the reflectance spectra may be analysed to identify the various vanadium species and to gain information on their dispersion state. The bands are broad, however, and in spectra containing several species overlapping bands may prevent a firm conclusion. In our sam-
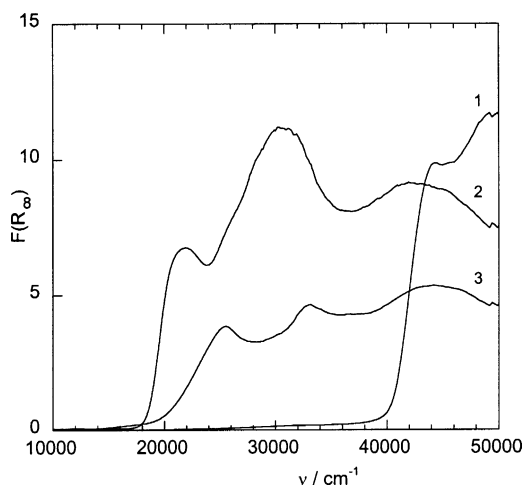
Fig. 3. Reflectance spectra for reference compounds: (1) $ZrO_2(823)$, y ($y = 2.7$ or 10); (2) V_2O_5; (3) ZrV_2O_7.

ples, the leaching experiment helped to assess the presence of V_2O_5 or vanadia-like polymers.

For the more dilute $ZVx,10$ samples ($x < 0.99$), for which no soluble vanadium was detected, we assigned the broad band at $36,000\,cm^{-1}$ (Fig. 4) to VO_x species, considered as the predominant species anchored to the zirconia surface. For samples with x in the range from 0.99 to 3.10 wt.%, the shifts in the maximum position to lower energy ($34,000\,cm^{-1}$) and the absorption edge to $20,000$–$18,000\,cm^{-1}$ suggest an increasing fraction of more condensed vanadium species interacting with the support and V_2O_5. Whether ZrV_2O_7 (bands at 25,000, 33,000 and $44,000\,cm^{-1}$, absorption edge at $18,000$–$19,000\,cm^{-1}$, Fig. 3) also formed remains unclear. All the vanadium species were nevertheless present as small (two or three dimensional) clusters, in agreement with the X-ray diffraction and XPS deduction. For higher vanadium content, these clusters increased in number or in size as indicated by the higher intensity of the absorption band in
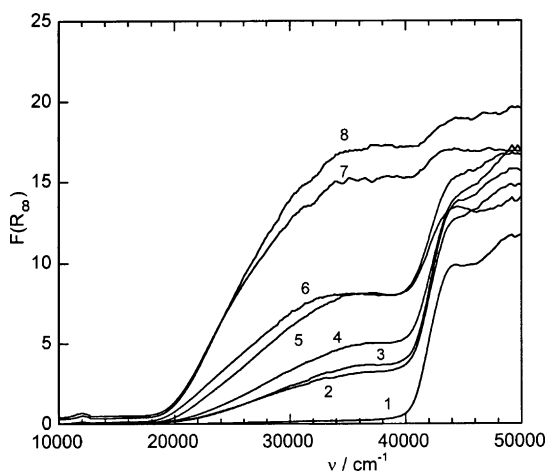
Fig. 4. Reflectance spectra for $ZVx,10$ samples: (1) $ZrO_2(823),10$; (2) ZV0.27,10; (3) ZV0.50,10; (4) ZV0.99,10; (5) ZV1.99,10; (6) ZV3.10,10; (7) ZV6.41,10; (8) ZV6.91,10.
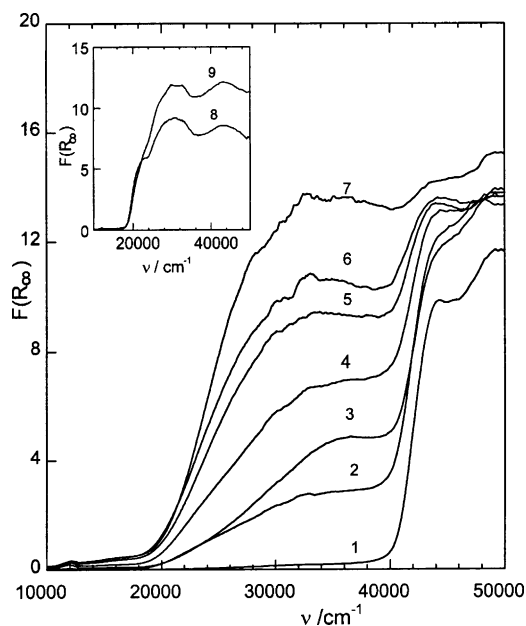
Fig. 5. Reflectance spectra for $ZVx,2.7$ samples: (1) $ZrO_2(823),2.7$; (2) ZV0.50,2.7; (3) ZV1.40,2.7; (4) ZV2.82,2.7; (5) ZV3.74,2.7; (6) ZV4.74,2.7; (7) ZV5.57,2.7; (8) ZV16.70,2.7; (9) ZV22.44,2.7.

the $20,000$–$35,000\,cm^{-1}$ region. Analogous results were reported recently by Male et al. [39] who studied zirconia-supported vanadia prepared by a thermolytic molecular route and heated as in the present study (823 K, for 3 h in air). They corroborated their UV–vis reflectance data with ^{51}V NMR and Raman spectroscopy.

The samples prepared at pH 2.7 contained a higher fraction of vanadium as condensed species. Compared with ZV0.5,10, the most dilute sample (ZV0.5,2.7), in addition to the absorption at $36,000\,cm^{-1}$ (presence of anchored VO_x species), Fig. 5, exhibited a relatively high absorption intensity in the region around $25,000\,cm^{-1}$, where both ZrV_2O_7 and V_2O_5 absorb, revealing the presence of these compounds. As the vanadium concentration increased, the rise in the absorption intensity in the low energy side indicated an increasing fraction of vanadium as ZrV_2O_7 or as V_2O_5, or both (Fig. 5).

The interaction of vanadium species with the zirconia surface, affects some solid state processes of the support, including phase transition and sintering. The protective effect against the decrease in the zirconia surface and the hindering of the phase transition (ZrO_2-t $\rightarrow$ ZrO_2-m), is well documented in the literature for various species [13,16,17,40] including vanadium [39,41]. Owing to the interaction of the surface species, these phenomena have been ascribed to the formation of surface compounds resulting in a decrease in the atomic mobility of the support surface. Phase transition and sintering differently depend on the interacting vanadium content. To rationalize the phase transition we recall that the hydrous zirconium oxide used as a starting material is formed by very small regions with a tetragonal structure [42]. When the hydrous zirconium oxide is heated, the tetragonal crystallites grow and, during the subsequent cooling, transform to
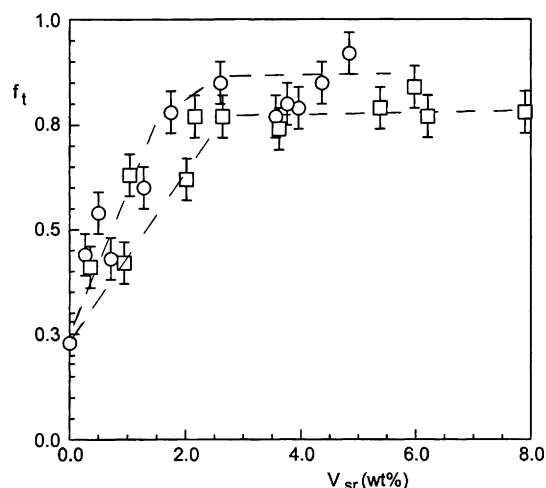
Fig. 6. Fraction of tetragonal zirconia, f_t, as a function of the vanadium content in the solid residue, V_{sr}: (○) ZVx,10; (□) ZVx,2.7.

the monoclinic phase [43], the thermodynamic stable phase in the temperature range used. The transformation starts at the particle surface and progresses inwards toward the centre of the crystalline particles [44,45]. In the presence of interacting species, the phase transition is hindered and the tetragonal form maintained. In our experiments, irrespective of the preparation pH, f_t reached its maximum values for $V_{sr} \approx 2$ wt.% and then remained constant (Fig. 6).

This finding suggests that the phase transition is mostly affected by highly dispersed species. Moreover, the f_t values for the ZVx,10 samples, systematically higher than those for ZVx,2.7, are related to the higher fraction of dispersed vanadium in the set prepared at basic pH.

Heating markedly decreased the surface area of vanadium-free zirconia (Table 1). In both series of samples, the $S(ZrO_2)$ values strongly increased with the vanadium remaining in the solid residue, V_{sr}, up to ~1 wt.%; the increase then continued but the slope became smaller, Fig. 7. For all ZVx,10 samples,
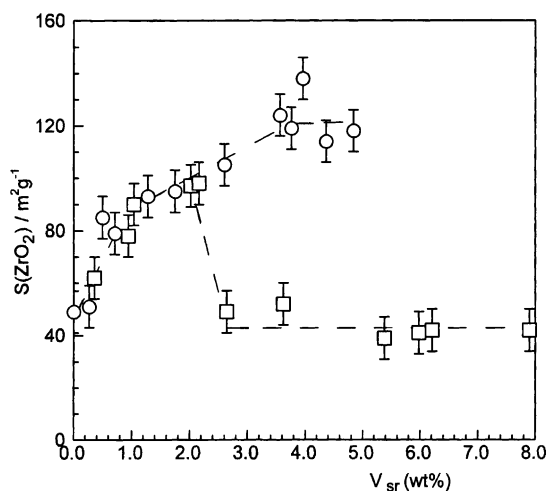
Fig. 7. Specific surface area of ZrO$_2$, $S(ZrO_2)$, as a function of the vanadium content in the solid residue, V_{sr}. (○) ZVx,10; (□) ZVx,2.7.
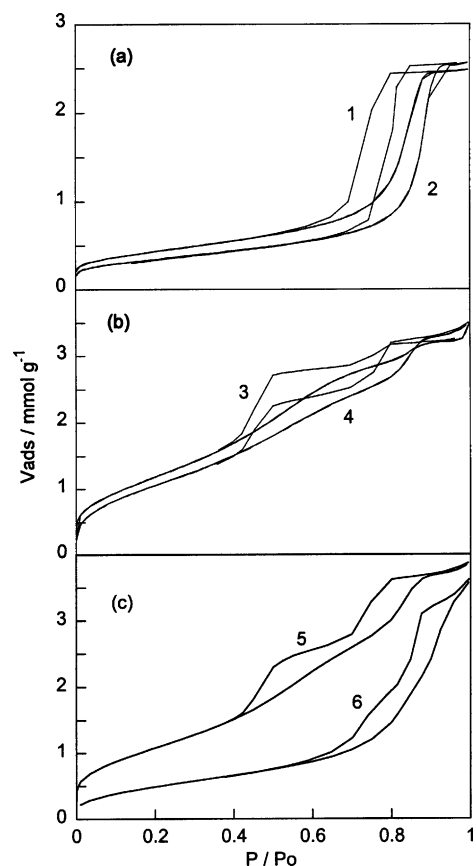
Fig. 8. Nitrogen adsorption–desorption isotherms at 77 K for typical ZV$x,y$ samples. (a) 1 — ZrO$_2$(823),2.7; 2 — ZrO$_2$(823),10. (b) 3 — ZV3.10,10; 4 — ZV5.14,10. (c): 5 — ZV2.82,2.7; 6 — ZV4.74,2.7.

the protective effect was present up to the most concentrated sample, reaching a value of 120 m^2 g^{-1} for $V_{sr} \sim 4$ wt.% and then remaining constant. For the ZVx,2.7 set, starting from $V_{sr} \sim 2.2$ wt.%, $S(ZrO_2)$ suddenly decreased to the value measured for vanadium-free ZrO$_2$. Accordingly, this series of samples contained a high fraction of vanadium present as V$_2$O$_5$ that in part reacted with ZrO$_2$ giving ZrV$_2$O$_7$ (detected by X-ray diffraction from ZV3.74,2.7, Table 1). Decreasing the interacting vanadium removed the protection against sintering.

The reaction between V$_2$O$_5$ and ZrO$_2$ nonetheless explains why the ZVx,2.7 samples, with $x \geq 3.74$, contained a smaller amount of leached vanadium than samples of the ZVx,10 series with similar vanadium content, Fig. 1, because ammonia dissolved hardly any ZrV$_2$O$_7$.

The strong change in the surface area involves a strong change in the texture. Compared with the ZrO$_2$(823), Fig. 8 (a), the presence of vanadium induces a change in adsorption–desorption isotherms depending on the vanadium concentration and preparation pH (Fig. 8 (b, c)). ZVx,10 ($x = 3.10$; 5.14) and ZVx,2.7 ($x = 2.82$; 4.74), as typical samples, yielded type IV isotherms in the BDDT classification [46] indicating mesoporous adsorbents. However, the shape of the hysteresis loops for the ZVx,2.7 and ZVx,10 samples
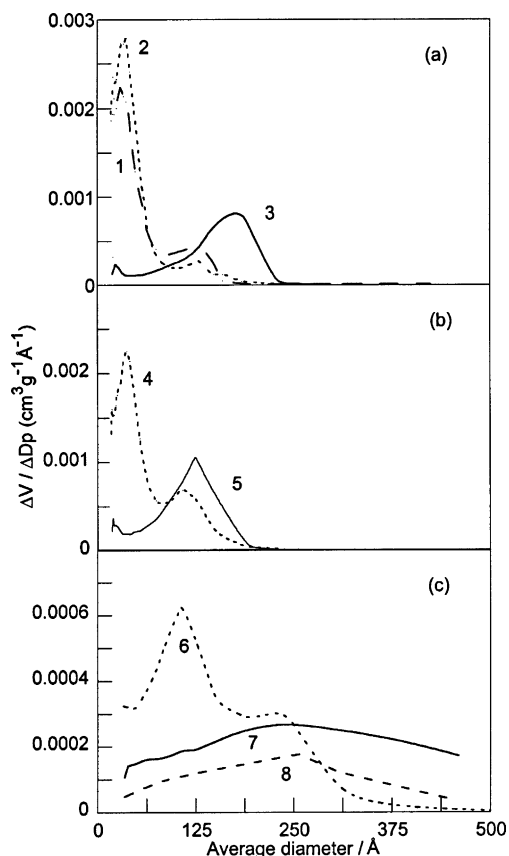
Fig. 9. BJH pore size distributions for typical ZVx,y samples. (a) 1 — ZV3.10,10; 2 — ZV5.14,10; 3 — ZrO_2,10(823). (b): 4 — ZV2.82,2.7; 5 — ZrO_2(823),2.7. (c): 6 — ZV4.74,2.7; 7 — ZV8.32,2.7; 8 — ZV22.24,2.7.

differed from that of ZrO_2(823)y (particularly the desorption branches) (Fig. 8 (a–c)) and the starting point of the hysteresis loop for ZVx,10 samples and ZV2.82,2.7 (P/Po around 0.4) was much lower than that of ZV4.74,2.7 and of ZrO_2(823)y (P/Po around 0.7).

Pore size analysis, following the BJH method [47], revealed a typical unimodal distribution in the mesopore range (120–180 Å) for ZrO_2(823)y samples and a bimodal or unimodal distribution for the vanadium-containing samples (Fig. 9 (a–c)). ZrO_2(383) is microporous with a pore-size distribution around 20 Å [16]. Heating caused the texture of ZrO_2(383) to evolve into a mesoporous organization with a pore-size distribution in the range 120–180 Å, Fig. 9 (a, b). For the ZVx,10 samples and for ZV2.82,2.7 the bimodal distribution was characterized by pore sizes around 30–40 and 110–130 Å. The ZV4.74,2.7 sample contained two pore families with sizes around 110 and 220 Å, whereas the more concentrated samples (ZV8.32,2.7 and ZV22.24,2.7) showed a very broad distribution with pore size centred around 230 Å, (Fig. 9 (c)). This behaviour suggests that the pore group with size around 30 Å derives from the fraction of zirconia strongly interacting with the vanadium species, and thus resembles the microporous structure of hydrous zirconia, whereas that around 120 Å comes from the non-interacting zirconia. The fact that the ZV2.82,2.7 sample, Fig. 9 (b), exhibited a

pore-size distribution curve similar to those observed for the ZVx,10 samples confirms that this sample contains a large fraction of dispersed and interacting vanadium species. Conversely, for higher vanadium loading (ZV4.74,2.7) the formation of V_2O_5 led to massive ZrV_2O_7 and the fraction of zirconia, no-longer protected, evolved towards a mesoporous structure resembling that of vanadium-free zirconia, Fig. 9 (c). The broad pore family with size around 230 Å, which becomes predominant at increasing vanadium loading (ZV8.32,2.7 and ZV22.24,2.7), is probably related to the formation of ZrV_2O_7 and V_2O_5.

4. Conclusions

Zirconia-supported vanadium oxide samples, obtained by heating at 823 K for 5 h in air precursors prepared by equilibrium adsorption at pH 10 (ZVx,10) or at pH 2.7 (ZVx,2.7), behave differently.

XRD, XPS and reflectance spectroscopy indicate that for similar vanadium content the degree of dispersion of the supported species is higher for ZVx,10 than for ZVx,2.7 samples. The powder patterns of ZVx,10 samples show no lines other than those of monoclinic and tetragonal ZrO_2. By contrast, the powder patterns of ZVx,2.7 samples show ZrV_2O_7 and V_2O_5 lines: ZrV_2O_7 starting from $x = 3.74$ and, ZrV_2O_7 and V_2O_5 from 8.38. The more dilute ZVx,10 samples ($x < 0.99$) predominantly contain VO_x species, anchored to the zirconia surface. As the vanadium content increases more condensed species involving ZrO_2 and V_2O_5 form as small clusters. Compared with samples of the ZVx,10 set, those prepared at pH 2.7 contain a higher fraction of vanadium as ZrV_2O_7 and V_2O_5.

The interaction of the dispersed vanadium species hinders the sintering and phase transition of the support. For ZVx,10 and for ZVx,2.7, x up to 2.82, the interacting vanadium preserves a fraction of zirconia with narrow pores (30 Å) whereas at higher loading the formation of ZrV_2O_7 and V_2O_5 removes the interacting vanadium and the support sinters.

References

[1] B.M. Weckhuysen, D.E. Keller, Catal. Today 78 (2003) 25.
[2] X. Gao, J.-M. Jehng, I.E. Wachs, J. Catal. 209 (2002) 43.
[3] J.-F. Lambert, M. Che, J. Mol. Catal. A 162 (2000) 5.
[4] A. Christodoulakis, M. Machli, A.A. Lemonidou, S. Boghosian, J. Catal. 222 (2004) 293.
[5] C.L. Pieck, M.A. Bañares, J.L.G. Fierro, J. Catal. 224 (2004) 1.
[6] M. De, D. Kunzru, Catal. Lett. 96 (2004) 33.
[7] M.L. Fereira, M.J. Volpe, J. Mol. Catal. A 184 (2002) 349.

[8] J.R. Sohn, I.J. Doh, Y.I. Pae, Langmuir 18 (2002) 6280.

[9] M. Kantcheva, Solid State Ionics 141/142 (2001) 487.

[10] G. Martra, F. Arena, S. Coluccia, F. Frusteri, A. Parmaliana, Catal. Today 63 (2000) 197.

[11] X. Gao, I.E. Wachs, J. Phys. Chem. B 104 (2000) 1261.

[12] B. Olthof, A. Khodakov, A.T. Bell, E. Iglesia, J. Phys. Chem. B 104 (2000) 1516.

[13] M. Valigi, D. Gazzoli, I. Pettiti, G. Mattei, S. Colonna, S. De Rossi, G. Ferraris, Appl. Catal. A 231 (2002) 159.

[14] S. De Rossi, G. Ferraris, M. Valigi, D. Gazzoli, Appl. Catal. A 231 (2002) 173.

[15] M. Scheithauer, C.-K. Cheung, R.E. Jentoft, R.K. Grasselli, B.C. Gates, H. Knözinger, J. Catal. 180 (1998) 1.

[16] A. Cimino, D. Cordischi, S. De Rossi, G. Ferraris, D. Gazzoli, V. Indovina, G. Minelli, M. Occhiuzzi, M. Valigi, J. Catal. 127 (1991) 744.

[17] M. Valigi, A. Cimino, D. Cordischi, S. De Rossi, G. Ferraris, D. Gazzoli, V. Indovina, G. Minelli, M. Occhiuzzi, Solid State Ionics 63–65 (1993) 136.

[18] M. Valigi, D. Gazzoli, A. Cimino, E. Proverbio, J. Phys. Chem. B 103 (1999) 11318.

[19] M. Valigi, D. Gazzoli, S. De Rossi, G. Ferraris, E. Bemporad, Phys. Chem. Chem. Phys. 5 (2003) 4974.

[20] M. Sanati, A. Andersson, L.R. Wallenberg, B. Rebenstorf, Appl. Catal. 106 (1993) 51.

[21] International, Centre for Diffraction Data, Data Sets 1–50 plus 70–88; Newtown Square, PA, USA 2000. Card. 41–1426.

[22] (a) G. Peyronel, Gazz. Chim. Ital. 72 (1942) 83;
(b) J.S. Evans, J.C. Hanson, A.W. Sleight, Acta Cryst. B 54 (1998) 705.

[23] P.E. Thomas, W.F. Pickering, Talanta 18 (1971) 127.

[24] D.R. Lide (Ed.), C.R.C. Handbook of Chemistry and Physics, 72nd ed., Chemical Rubber Publishing Company, Ann Arbor, 1992, p. 4–110.

[25] D. Briggs, J.C. Rivère, in: D. Briggs, M.P. Seah (Eds.), Practical Surface Analysis – Auger and X-Ray Photoelectron Spectroscopy, second ed., Wiley, Chichester, 1990, p. 127.

[26] A. Cimino, D. Gazzoli, M. Valigi, J. Electron Spectrosc. Relat. Phenom. 104 (1999) 1.

[27] F.P.J. Kerkhof, J.A. Moulijn, J. Phys. Chem. 83 (1979) 1612.

[28] J.E. Fulghum, R.W. Linton, Surf. Interface Anal. 13 (1988) 186.

[29] H. Scofield, J. Electron Spectrosc. Relat. Phenom. 8 (1976) 129.

[30] M.P. Seah, Surf. Interface Anal. 9 (1986) 85.

[31] M.P. Seah, Surf. Interface Anal. 20 (1993) 243.

[32] M. Kosmulski, J. Coll. Interf. Sci. 275 (2004) 214.

[33] S.I. Pechenyuk, S.I. Matveenko, V.V. Semushin, Russ. Chem. Bull., International Edition 50 (2001) 1582.

[34] G. Rasch, H. Bögel, C. Rein, Z. Chem. Phys. (Leipzig) 259 (1978) 955.

[35] M. Schraml-Marth, A. Wokaun, M. Pohl, H.-L. Krauss, J. Chem. Soc. Faraday Trans. 87 (1991) 2635.

[36] G. Lischke, W. Hanke, H.-G. Jerschkewitz, G.J. Öhlmann, J. Catal. 91 (1985) 54.

[37] R. Rulkens, J.L. Male, K.W. Terry, B. Olthof, A. Khodakov, A.T. Bell, E. Iglesia, T.D. Tilley, Chem. Mater. 11 (1999) 2966.

[38] R.S. Weber, J. Catal. 151 (1995) 470.

[39] J.L. Male, H.G. Niessen, A.T. Bell, T.D. Tilley, J. Catal. 194 (2000) 431.

[40] M. Valigi, A. Cimino, D. Gazzoli, G. Minelli, Solid State Ionics 32/33 (1989) 698.

[41] C.L. Pieck, M.A. Bañares, M.A. Vincente, J.L.G. Fierro, Chem. Mater. 13 (2001) 1174.

[42] J. Livage, K. Doi, C. Maziers, J. Am. Ceram. Soc. 51 (1968) 349.

[43] R. Srinivasan, B.H. Davis, O.B. Calvin, C.R. Hubbard, J. Am. Ceram. Soc. 75 (1992) 1217.

[44] J.R. Anderson, Structure of Metallic Catalysts, Academic Press, New York, 1975, p. 62.

[45] T. Isobe, M. Senna, J. Solid State Chem. 93 (1991) 368.

[46] S. Brunauer, L.S. Deming, W.S. Deming, E.J. Teller, J. Am. Chem. Soc. 62 (1940) 1723.

[47] E.P. Barrett, L.G. Joyner, P.P. Halenda, J. Am. Chem. Soc. 73 (1951) 373.